



## Article

# Structural, Electronic and Optical Properties of Some New Trilayer Van de Waals Heterostructures

Beitong Cheng <sup>1</sup>, Yong Zhou <sup>1,2</sup>, Ruomei Jiang <sup>1</sup>, Xule Wang <sup>1</sup>, Shuai Huang <sup>1</sup>, Xingyong Huang <sup>3</sup>, Wei Zhang <sup>1</sup>, Qian Dai <sup>1</sup>, Liujiang Zhou <sup>4</sup>, Pengfei Lu <sup>5,\*</sup> and Hai-Zhi Song <sup>1,4,6,\*</sup>

<sup>1</sup> Quantum Research Center, Southwest Institute of Technical Physics, Chengdu 610041, China; beitung20@163.com (B.C.)

<sup>2</sup> School of Electronic Engineering, Chengdu Technological University, Chengdu 611730, China

<sup>3</sup> Faculty of Science, Yibin University, Yibin 644007, China

<sup>4</sup> Institute of Fundamental and Frontier Sciences, University of Electronic Science and Technology of China, Chengdu 610054, China

<sup>5</sup> State Key Laboratory of Information Photonics and Optical Communications, Beijing University of Posts and Telecommunications, Beijing 100876, China

<sup>6</sup> State Key Laboratory of High Power Semiconductor Lasers, Changchun University of Science and Technology, Changchun 130013, China

\* Correspondence: lupengfei@bupt.edu.cn (P.L.); hzsong@uestc.edu.cn (H.-Z.S.); Tel.: +86-158-2823-9155 (H.-Z.S.)

**Abstract:** Constructing two-dimensional (2D) van der Waals (vdW) heterostructures is an effective strategy for tuning and improving the characters of 2D-material-based devices. Four trilayer vdW heterostructures, BP/BP/MoS<sub>2</sub>, BlueP/BlueP/MoS<sub>2</sub>, BP/graphene/MoS<sub>2</sub> and BlueP/graphene/MoS<sub>2</sub>, were designed and simulated using the first-principles calculation. Structural stabilities were confirmed for all these heterostructures, indicating their feasibility in fabrication. BP/BP/MoS<sub>2</sub> and BlueP/BlueP/MoS<sub>2</sub> lowered the bandgaps further, making them suitable for a greater range of applications, with respect to the bilayers BP/MoS<sub>2</sub> and BlueP/MoS<sub>2</sub>, respectively. Their absorption coefficients were remarkably improved in a wide spectrum, suggesting the better performance of photodetectors working in a wide spectrum from mid-wave (short-wave) infrared to violet. In contrast, the bandgaps in BP/graphene/MoS<sub>2</sub> and BlueP/graphene/MoS<sub>2</sub> were mostly enlarged, with a specific opening of the graphene bandgap in BP/graphene/MoS<sub>2</sub>, 0.051 eV, which is much larger than usual and beneficial for optoelectronic applications. Accompanying these bandgap increases, BP/graphene/MoS<sub>2</sub> and BlueP/graphene/MoS<sub>2</sub> exhibit absorption enhancement in the whole infrared, visible to deep ultraviolet or solar blind ultraviolet ranges, implying that these asymmetrically graphene-sandwiched heterostructures are more suitable as graphene-based 2D optoelectronic devices. The proposed 2D trilayer vdW heterostructures are prospective new optoelectronic devices, possessing higher performance than currently available devices.

**Keywords:** two-dimensional material; van der Waals heterostructure; trilayer; the first-principles calculation



**Citation:** Cheng, B.; Zhou, Y.; Jiang, R.; Wang, X.; Huang, S.; Huang, X.; Zhang, W.; Dai, Q.; Zhou, L.; Lu, P.; et al. Structural, Electronic and Optical Properties of Some New Trilayer Van de Waals Heterostructures. *Nanomaterials* **2023**, *13*, 1574. <https://doi.org/10.3390/nano13091574>

Academic Editor: Iván Mora-Seró

Received: 7 April 2023

Revised: 30 April 2023

Accepted: 5 May 2023

Published: 8 May 2023



**Copyright:** © 2023 by the authors. Licensee MDPI, Basel, Switzerland. This article is an open access article distributed under the terms and conditions of the Creative Commons Attribution (CC BY) license (<https://creativecommons.org/licenses/by/4.0/>).

## 1. Introduction

Van der Waals (vdW) heterostructures [1–3] containing different two-dimensional (2D) material monolayers have recently attracted interest for fundamental physics in low-dimensional systems [4–8] and for applications in microelectronic and optoelectronic devices [9–12]. Several kinds of typical 2D materials such as graphene [13–15], transition metal dichalcogenide (TMD) [16,17] and phosphorene [18–20] have been incorporated into this construction. In graphene/MoS<sub>2</sub>, good thermal stability with high atom cohesive energy was confirmed [21] and found to mainly be associated with vdW coupling [22], and an electric field applied at the hetero-interface can control the Schottky barriers and Ohmic contacts [23]. Bilayer graphene/black-phosphorous (BP) was proposed to protect

BP from its structural and chemical degradation with a slightly opened graphene band gap while still maintaining the electronic characteristics of graphene and BP monolayers [24,25]. Graphene/hexagonal-boron-nitride (hBN) appears to have good electric-field-driven switching, which is beneficial to the field-effect transistor [26]. MoS<sub>2</sub>/MX<sub>2</sub> (M = Mo, Cr, W; X = S, Se) bilayer heterostructures exhibit semiconductor properties with an indirect band gap, except for MoS<sub>2</sub>/WSe<sub>2</sub> [27], and all of them can undergo transiting from semiconductors to metals with the strain and band gap decreasing with the electric field [28], showing prospects for construction of ultrathin flexible devices and for application in viable optoelectronic fields. The TMD/BN heterostructures were explored for application in photocatalytic fields owing to the direct bandgap and powerful built-in electric field across the interface [29]. The type-II band alignments of MoS<sub>2</sub>/ZnO and WS<sub>2</sub>/ZnO help to separate the photo-generated charge effectively, and all TMD/graphene-like-ZnO structures show optical absorption in the visible and infrared regions [30]. Blue-phosphorous (BlueP)/BP possesses a tunable bandgap, band edges and electron-hole behavior by applying perpendicular electric field, and it thus shows potential for use in novel optoelectronic devices [31]. BlueP/GaN vdW heterostructure was found active for facilitating charge injection and thus promising for unipolar electronic device applications [32]. The photoelectric performances of BP/TMD heterostructures can be improved by applying compressive stress [33] or an electric field [34]. BP/MoS<sub>2</sub> demonstrated an improved response and absorption characteristics in photodetectors [35]. Many BP/XT<sub>2</sub> (X = Mo, W; T = S, Se, Te) heterostructures with type-II band alignments would be prospective as spin-filter devices [36]. BlueP/MoS<sub>2</sub> has been considered the next generation of photovoltaic devices and water-splitting materials due to its wide optical response range and good light absorption ability [37]. In addition to the theoretical research such as that mentioned above, there have been experimental studies on bilayer vdW heterostructures to explore their practical prospects. The BP/MoS<sub>2</sub> heterostructure photodetector was prepared and demonstrated with a wide range of current-rectifying behavior, microsecond response speed and high detectivity [38]. Graphene/BP heterostructure phototransistors exhibited good photoconductive gain and thus an ultrahigh photoresponse at near-infrared wavelength, implying the potential applications in remote sensing and environmental monitoring [39]. It is apparent that building vdW heterostructures is an effective way to achieve higher performance from devices based on graphene, phosphorenes and TMDs.

As an extension to the above idea, trilayer vdW heterostructures have recently been attracting more and more attention, since one more layer might open more space for tuning the properties further [40,41]. Simulation by Datta et al. demonstrated that the electronic properties of MoS<sub>2</sub>/MX<sub>2</sub>/MoS<sub>2</sub> exhibit a smaller electron effective mass and a semiconductor-to-metal transition under tensile strain [42]. Device level performance of MoS<sub>2</sub>/MX<sub>2</sub>/MoS<sub>2</sub> were further calculated, showing that these trilayer heterostructures would be prospective to construct highly sensitive field effect transistors for nanobiomolecules sensing as well as for pH sensing [43]. Bafekry et al. theoretically analyzed trilayer vdW heterostructures in which MoS<sub>2</sub> monolayer is encapsulated by two graphitic carbon nitride monolayers, revealing their magnetic metallic characteristics [44] probably applicable in nano-spintronic devices. Liu et al. proposed trilayer heterostructures MoS<sub>2</sub>/SiC/MoS<sub>2</sub> and SiC/MoS<sub>2</sub>/SiC, and predicted their strain-induced tunable band structure promising for future optoelectronic devices [45]. Calculation on BlueP/MoX<sub>2</sub>-based trilayer heterostructures demonstrated the excellent ability to accelerate the separation of photo-generated electron-hole pairs and the controllable power conversion efficiency indicating great potential for photocatalysis and photovoltaics [46]. BN/graphene/BN was proposed and simulated to open the graphene bandgap and enhance the application potential for radio-frequency devices and switching transistors [47,48]. Xu et al. theoretically argued that MoS<sub>2</sub>-graphene-based trilayer heterostructures are of unique optoelectronic properties tunable by external electric field and thus of great potential for solar energy harvesting and conversion [49]. External electric field modulation effects were also simulated on PtSe<sub>2</sub>/graphene/graphene and graphene/PtSe<sub>2</sub>/graphene, revealing their usefulness to

guide the design of high-performance field effect transistors [50]. In an experimental work, Long et al. fabricated WSe<sub>2</sub>/graphene/MoS<sub>2</sub> p-g-n heterostructure photodetector, which achieved a wide detection wavelength range of 400–2400 nm and a short rise/fall time [51]. Li et al. fabricated photodetectors based on dielectric shielded MoTe<sub>2</sub>/graphene/SnS<sub>2</sub> p-g-n junctions, and achieved extraordinary responsivity as high as 2600 A/W, detectivity as good as 10<sup>13</sup> Jones with fast photoresponse in the range of 405–1550 nm [52]. It is thus clear that constructing trilayer vdW heterostructures can improve further the performance of electronic and optoelectronic devices based on graphene, phosphorenes and TMDs. However, the reported trilayer heterostructures used mainly symmetrical structures and/or contained two types of materials. Further efforts should be made to construct new vdW heterostructures.

In this work, we attempt to construct and study trilayer vdW heterostructures with asymmetric structures and/or three different types of 2D materials. Four kinds of trilayer heterostructures containing MoS<sub>2</sub>, phosphorene and/or graphene are simulated in terms of structural, optical and optoelectronic properties. It is suggested that sophisticated 2D trilayer vdW heterostructures can provide further optimized characters for a new generation of optoelectronic devices.

## 2. Calculation Methods

In this study, we designed four trilayer vdW heterostructures BP/BP/MoS<sub>2</sub>, BlueP/BlueP/MoS<sub>2</sub>, BP/graphene/MoS<sub>2</sub> and BlueP/graphene/MoS<sub>2</sub>, which are structurally asymmetric and/or composed of more than two different types of 2D materials. The first-principles calculation was performed using the tool of Vienna ab initio simulation package (VASP) [53] within Density Functional Theory (DFT) and the projector-augmented wave (PAW) method [54]. The generalized gradient approximation (GGA) with the Perdew–Burke–Ernzerhof (PBE) method was applied for calculating electron exchange and correlation potentials [54,55]. Due to the weak vdW interaction between the monolayers, the opt-PBE vdW method [55,56] was adopted to modify the vdW dispersion. To avoid the interaction between adjacent slab models, the thickness of the vacuum layer was set to 20 Å. The energy cutoff, convergence criteria of total energy and force were set to 450 eV, 10<sup>−5</sup> eV and 0.01 eV/Å, respectively. When optimizing the trilayer atomic structures, 1 × 7 × 1, 3 × 3 × 1, 2 × 2 × 1 and 3 × 3 × 1 k-point sets were adopted for BP/BP/MoS<sub>2</sub>, BlueP/BlueP/MoS<sub>2</sub>, BP/graphene/MoS<sub>2</sub> and BlueP/graphene/MoS<sub>2</sub>, respectively. When calculating the electronic structures, 5 × 21 × 1, 16 × 16 × 1, 5 × 5 × 1 and 8 × 8 × 1 k-point sets were adopted for the four structures, respectively. When calculating the optical properties, 8 × 21 × 1, 20 × 20 × 1, 10 × 10 × 1 and 13 × 13 × 1 k-point sets were adopted for the four structures, respectively. The above-mentioned k-point sets were actually determined by convergence tests: increasing the k-point set scale until a state in which the calculation results do not change beyond the convergence standard any longer. It reflects that calculations for structural, electronic and optical properties need more and more computational cost and accuracy.

To establish the stability of the proposed vdW heterostructures, we should in principle evaluate their vibrational frequencies to seek real and positive phonon parameters. Nevertheless, most of the first-principles simulations on vdW heterostructures took the binding energy as the figure of merit to characterize the structure stability [21,27,30,36], because the vibrations are so computationally expensive that a complex structure would be technically hard to deal with. In our case, the proposed atomic structures are even larger and complicated, so we judge the structure stability and thus the experimental feasibility by calculating the binding energy, which would be negative for a stable system [23]. The binding energy ( $E_b$ ) is calculated using the following equation:

$$E_b = E_{\text{hts}} - E_A - E_B - E_C \quad (1)$$

where  $E_{\text{hts}}$  represents the overall energy of the heterostructure and  $E_A$ ,  $E_B$ , and  $E_C$  represent the energy of each monolayer in its free state. The work function, used as the key parameter to deduce the band alignment, is described by

$$W = E_{\text{vac}} - E_f \quad (2)$$

where  $E_{\text{vac}}$  is the energy of a stationary electron in the vacuum and  $E_f$  is the Fermi level.

The macroscopic optical response function is usually measured by the complex dielectric function  $\varepsilon(\omega) = \varepsilon_1(\omega) + i\varepsilon_2(\omega)$ , where  $\omega$  represents the circular frequency of light. The real part  $\varepsilon_1(\omega)$  can be processed via the Kramers–Kronig relation and the imaginary part  $\varepsilon_2(\omega)$  is produced by Fermi's golden rule [57]. Based on these parameters, we can obtain the absorption coefficient by [58],

$$\alpha(\omega) = \frac{\sqrt{2}\omega}{c} \{[\varepsilon_1^2(\omega) + \varepsilon_2^2(\omega)]^{1/2} - \varepsilon_1(\omega)\}^{1/2} \quad (3)$$

### 3. Results and Discussion

#### 3.1. Structural Parameters

Due to the surface relaxation and interfacial mismatch, the trilayer vdW heterostructure supercells must be carefully set, for which we here extend monolayer cells individually to satisfy the length matching between different layers. The BP/BP/MoS<sub>2</sub> heterostructure is constructed from a  $4\sqrt{3} \times 1$  supercell MoS<sub>2</sub> monolayer and a  $5 \times 1$  supercell bilayer-BP, while the BlueP/BlueP/MoS<sub>2</sub> heterostructure is formed by stacking a  $3 \times 3$  supercell bilayer-BlueP on a  $3 \times 3$  supercell MoS<sub>2</sub> monolayer. After structure optimization calculation, we obtain the rectangular lattice constants  $a = 22.227$  and  $b = 3.278$  Å for BP/BP/MoS<sub>2</sub>, and the hexagonal lattice constants  $a = b = 9.642$  Å for BlueP/BlueP/MoS<sub>2</sub>. For BP/graphene/MoS<sub>2</sub>, bilayer BP/graphene cells are first constructed by matching  $3 \times 1$  BP with  $4\sqrt{3} \times 1$  supercell graphene, and then the  $1 \times 2$  supercell of the bilayer BP/graphene is set to match the  $2\sqrt{3} \times 3$  supercell MoS<sub>2</sub>. For BlueP/graphene/MoS<sub>2</sub>, a  $3 \times 3$  supercell monolayer BlueP,  $4 \times 4$  supercell graphene, and  $3 \times 3$  supercell monolayer MoS<sub>2</sub> are successively stacked. The optimized rectangular lattice constants of BP/graphene/MoS<sub>2</sub> are  $a = 10.256$  Å and  $b = 8.907$  Å, and the hexagonal ones of BlueP/graphene/MoS<sub>2</sub> are  $a = b = 9.776$  Å. The simulated models of BP/BP/MoS<sub>2</sub>, BlueP/BlueP/MoS<sub>2</sub>, BP/graphene/MoS<sub>2</sub> and BlueP/graphene/MoS<sub>2</sub> are depicted in Figure 1.

The trilayer vdW heterostructures will have different energies with different layer spacing. Figure 1 gives the layer spacing when the system reaches the final equilibrium. The calculated binding energy of the four trilayer heterostructures is  $-21.12$ ,  $-65.41$ ,  $-21.92$  and  $-65.78$  eV, respectively. The negative binding energies indicate that all the four proposed vdW heterostructures are structurally highly stable like the reported bilayer heterostructures [21,36]. The structure stability may imply the fabrication feasibility to some degree. As is known, BP/MoS<sub>2</sub> [38], graphene/MoS<sub>2</sub> [59], graphene/BP [39] bilayer heterostructures, and TMD/graphene/MoS<sub>2</sub> [51] trilayer heterostructures have been successfully fabricated using physical and chemical methods including mechanical stripping, liquid-phase stripping, hydrothermal and chemical vapor deposition. BlueP 2D monolayer has been well fabricated by molecular beam epitaxy [60], and the possibility to form its heterostructure with other 2D materials has been stated by a few studies [37,46]. Combining together the above fabrication abilities and considering the confirmed structure stability, the preparation of our proposed vdW heterostructures will be experimentally feasible. Noting the binding energy differences among these heterostructures, BlueP/BlueP/MoS<sub>2</sub> and BlueP/graphene/MoS<sub>2</sub> might be easier to be fabricated than BP/BP/MoS<sub>2</sub> and BP/graphene/MoS<sub>2</sub>, although BlueP-related 2D materials seem currently farther away from practical manufacture than BP-related ones.

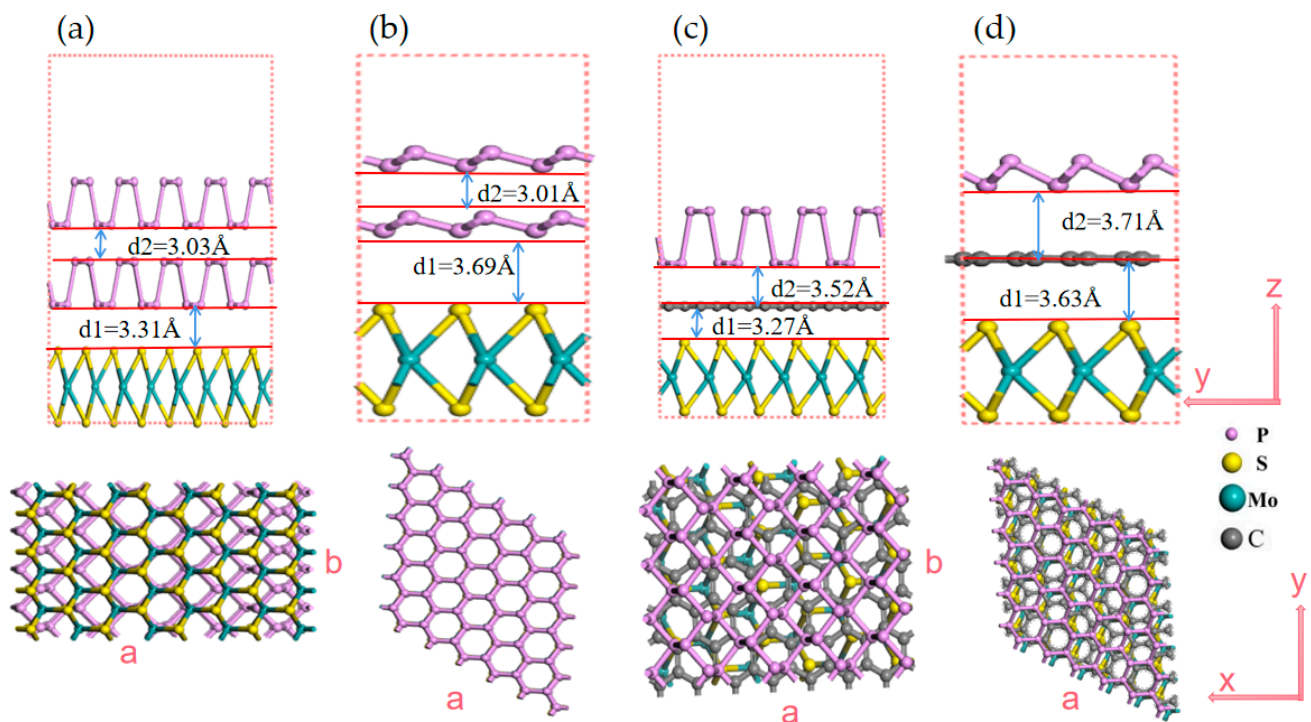


**Figure 1.** The models of trilayer 2D vdW heterostructures. (a) BP/BP/MoS<sub>2</sub>; (b) BlueP/BlueP/MoS<sub>2</sub>; (c) BP/graphene/MoS<sub>2</sub>; (d) BlueP/graphene/MoS<sub>2</sub>.

### 3.2. Electronic Properties

#### 3.2.1. Band Structure

Figure 2a,b demonstrate the projected band structures of BP/BP/MoS<sub>2</sub> and BlueP/BlueP/MoS<sub>2</sub> calculated using the PBE method. BP/BP/MoS<sub>2</sub> exhibits the conduction band minimum (CBM) located between the Y and G points and mostly contributed by MoS<sub>2</sub> (red lines) as well as the valance band maximum (VBM) located at the high-symmetry G point and mostly contributed by BP (blue lines). These are qualitatively consistent with our calculation of the bilayer counterpart BP/MoS<sub>2</sub> (in agreement with [34]), suggesting that the high hole mobility of BP and high electron mobility of MoS<sub>2</sub> are still preserved. The indirect bandgap of the  $4\sqrt{3} \times 1$  supercell MoS<sub>2</sub>, 1.338 eV, and the direct bandgap of the  $5 \times 1$  supercell bilayer-BP, 0.706 eV, are reduced compared with those in bilayer BP/MoS<sub>2</sub> (MoS<sub>2</sub> 1.398 eV, BP 0.876 eV), which are already lower than the free monolayer ones (MoS<sub>2</sub> 1.69 eV, BP 0.9 eV [36]). Significantly, the whole BP/BP/MoS<sub>2</sub> heterostructure possesses an indirect band gap of 0.167 eV, nearly half that of bilayer BP/MoS<sub>2</sub>, 0.326 eV. It is seen that this trilayer heterostructure effectively tunes the bandgap further. For BlueP/BlueP/MoS<sub>2</sub>, the CBM is located between the G and M points and is also mostly contributed by MoS<sub>2</sub> (red lines), whereas the VBM is located at the high-symmetry K point and is mostly contributed by BlueP (blue lines), consistent with the calculated results of the bilayer counterpart BlueP/MoS<sub>2</sub> (in agreement with [37]). Similar to the above BP/BP/MoS<sub>2</sub>, the direct bandgap of the  $3 \times 3$  supercell MoS<sub>2</sub> monolayer, 1.298 eV, and the indirect bandgap of the  $3 \times 3$  supercell BlueP monolayer, 1.624 eV, are smaller than those in the bilayer BlueP/MoS<sub>2</sub> (MoS<sub>2</sub> 1.328 eV, BlueP 1.698 eV), which are already decreased compared with the corresponding free monolayer ones (MoS<sub>2</sub> 1.69 eV, BlueP 1.908 eV [2,37]). The whole trilayer heterostructure possesses an indirect band gap of 1.2632 eV, smaller than that of the bilayer BlueP/MoS<sub>2</sub>, 1.3746 eV. It falls in between the BlueP/MoS<sub>2</sub>/BlueP of 1.013 eV and MoS<sub>2</sub>/BlueP/MoS<sub>2</sub> of 1.561 eV reported by Han et al. [46], again implying the further effective tuning by such an asymmetric trilayer heterostructure. The BP(BlueP) and MoS<sub>2</sub> bandgap decrease as they compose bilayer or trilayer heterostructures, which can be attributed to  $\sim 2.5\%$  and  $\sim 2\%$  lattice mismatch and a weak vdW force [35]. A whole-bandgap

decrease with the addition of a BP(BlueP) monolayer was discovered by Dong et al. and Qiao et al. in their studies on BP [57,61]; bandgap engineering by means of the simple addition of monolayers appears thus to be effective. Moreover, it is interesting here that the VBM of BlueP and MoS<sub>2</sub> are becoming much closer, which supports application with the function of carrier transferring or tunneling.

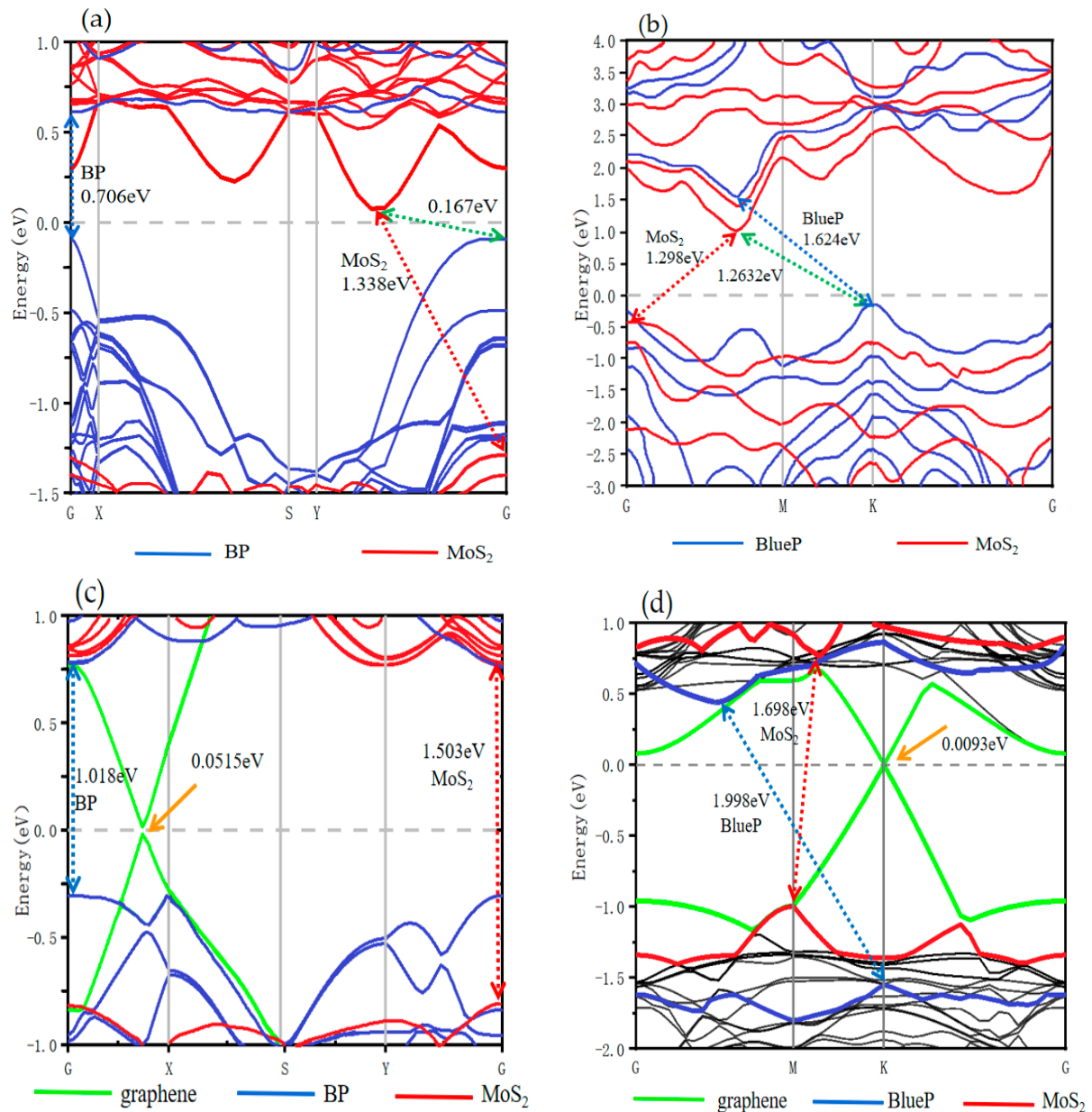


**Figure 2.** Calculated projected band structures for trilayer vdW heterostructures (a) BP/BP/MoS<sub>2</sub>; (b) BlueP/BlueP/MoS<sub>2</sub>; (c) BP/graphene/MoS<sub>2</sub>; (d) BlueP/graphene/MoS<sub>2</sub>. The Fermi level  $E_f$  is set as zero energy.

Figure 2c,d show the projected band structure of BP/graphene/MoS<sub>2</sub> and BlueP/graphene/MoS<sub>2</sub> trilayer vdW heterostructures calculated using the PBE method. What is immediately significant is that the BP/graphene/MoS<sub>2</sub> structure opens the bandgap of graphene to 0.051 eV, which is over one order of magnitude larger than the opening by the reported bilayer heterostructures such as graphene/BP (~0.0013 eV) [24], graphene/ZnO (~0.0057 eV) [30], and graphene/MoS<sub>2</sub> (~0.0007 eV) [49], and remarkably larger than those by other trilayer heterostructures such as graphene/ZnO/MoS<sub>2</sub> (~0.0048 eV) [30], graphene/nitrogen/graphene (~0.04 eV) [40], and graphene/BN/graphene

( $\sim 0.020$  eV) [47]. BlueP/graphene/MoS<sub>2</sub> opens the bandgap of graphene by 0.0093 eV, similar to many other heterostructures. The effectiveness of the graphene bandgap opening in BP/graphene/MoS<sub>2</sub> can hardly be attributed to strain, because the strains of graphene in both structures are close to each other (3.2% and 2.8%) and close to those of the reported structures such as graphene/BP (3%) [24]. We believe it originates from the united vdW coupling forces among BP and MoS<sub>2</sub> monolayers and possible built-in electric fields. The remarkable graphene bandgap opening suggests potential applications in temperature-sensitive devices [62]. On the basis of guaranteeing the excellent electronic properties of graphene, it can also be applied to field effect transistors with a high switching ratio. It is worth noting that these band gap values are grossly underestimated owing to adopting PBE functional calculation, so the real bandgaps of graphene in such heterostructures may be larger to match more extended application prospects. Furthermore, the band gap values of BP ( $\sim 1.018$  eV) and BlueP ( $\sim 1.998$  eV) in these two trilayer heterostructures are, qualitatively as graphene does, slightly larger than the free monolayers (BP of 0.9 eV [36] and BlueP of 1.908 [37]), which is in contrast to the first two structures BP/BP/MoS<sub>2</sub> and BlueP/BlueP/MoS<sub>2</sub>. There seem to be two types of bandgap engineering mechanisms in trilayer vdW heterostructures, providing wider space for novel device design.

We also calculated the local density of state (LDOS) and total density of states (TDOS) of BP/BP/MoS<sub>2</sub> and BlueP/BlueP/MoS<sub>2</sub>, as shown in Figure 3. The CBM state is mainly contributed by the Mo element and the VBM state relies on the P element, but the small difference between LDOS and TDOS may suggest that the interlayer vdW interaction also has a role in tuning the energy bands. What is quite significant is that only one more monolayer of BP(BlueP) increases the DOS to more than twice compared with the corresponding bilayer heterostructures. A similar phenomenon occurs in BP/graphene/MoS<sub>2</sub> and BlueP/graphene/MoS<sub>2</sub>, where the DOS also increases due to the insertion of a single graphene monolayer with respect to BP/MoS<sub>2</sub> and BlueP/MoS<sub>2</sub> bilayer heterostructures. It evidences the effectiveness of the proposed trilayer vdW heterostructures in optimizing the performance of 2D material systems.

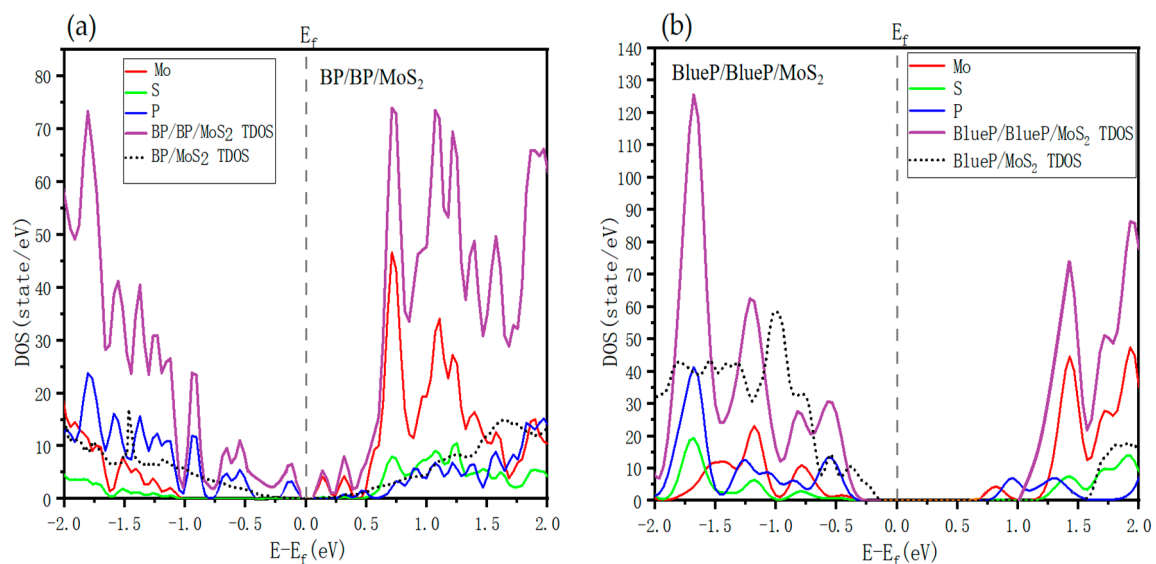


**Figure 3.** Calculated LDOS and TDOS for (a) BP/BP/MoS<sub>2</sub> and (b) BlueP/BlueP/MoS<sub>2</sub>. The different colors represent different elements. The gray dashed line indicates Fermi energy. That of bilayer counterpart is also shown for comparison.

### 3.2.2. Band Alignment

The band alignment of the vdW heterostructure is important in the design of new 2D-material structures. It is thus necessary to specifically pick up the band alignment data from the proceeding band structures with the help of calculating the work func-

tion. In Figure 4, for the BP/BP/MoS<sub>2</sub> and BlueP/BlueP/MoS<sub>2</sub> heterostructures, p-type bilayer-BP(BlueP) ( $E_f$  closer to VBM) and n-type MoS<sub>2</sub> ( $E_f$  closer to CBM) form type-II band alignment, as is expected. This band alignment has carrier confinement effects [63], favoring the electron-hole separation and then increasing the internal gain and responsivity of photodetectors. In brief, BP/BP/MoS<sub>2</sub> shows a more obvious type-II band alignment with a larger offset on the valence band and will produce a stronger carrier confinement effect compared with BP/MoS<sub>2</sub> [37,40]. With graphene inserted, BP/graphene/MoS<sub>2</sub> and BlueP/graphene/MoS<sub>2</sub> heterostructures naturally show a type-I quantum-well-like band alignment, providing the potential to construct nano-scaled bipolar transistors, field-effect transistors and photon transistors, which may need three different energy structures. In contrast to the Schottky contact of graphene/MoS<sub>2</sub> and graphene/BP(BlueP), here, semiconductor heterojunctions are formed. By applying an electric field across this semiconductor heterojunction, the graphene bandgap can be further flexibly tuned to exhibit different band alignments, which is of significance for the construction of new types of field-effect photodetectors [49].

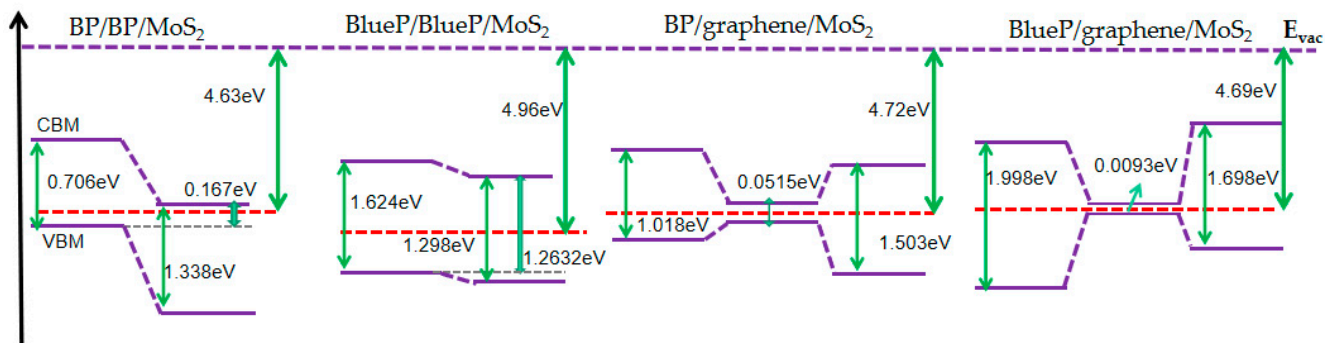


**Figure 4.** Band alignments of BP/BP/MoS<sub>2</sub>, BlueP/BlueP/MoS<sub>2</sub>, BP/graphene/MoS<sub>2</sub> and BlueP/graphene/MoS<sub>2</sub>. The red dashed lines represent the Fermi levels. The vacuum level ( $E_{vac}$ ) is shown by a purple dashed line.

### 3.3. Optical Absorption Spectra

On the optical absorption properties of 2D materials, many studies have been devoted to monolayer and bilayer vdW heterostructures, but little research has been carried out on trilayer ones, let alone a comparison between the bilayer and trilayer heterostructures [48]. The absorption spectra of BP/BP/MoS<sub>2</sub> and BlueP/BlueP/MoS<sub>2</sub> trilayer heterostructures are shown in Figure 5a,b. The absorption edge redshifts effectively expand the application ranges from covering the short-wave infrared band to covering the mid-wave infrared band for BP-based material, and from covering the visible band to covering the short-wave infrared band for BlueP-based material. This change is directly associated with the shrinkage of the bandgaps observed in Figure 3, but there seems to be something more incorporated as we see the following. Obviously, with only one more phosphorene monolayer, i.e.,  $\sim 1/3$  increase in material quantity, the spectral absorption intensity increases to be more or less twice with respect to monolayer and bilayer counterparts. This is more than expected, meaning that these two trilayer heterostructures greatly improve the quantum efficiency in optoelectronic devices [64] in wide spectral ranges. This sort of enhancement might be the result of complex interlayer vdW interactions. In more detail, the absorption of BP/BP/MoS<sub>2</sub> is much stronger (reaching  $10^5 \text{ cm}^{-1}$ ) than that of BlueP/BlueP/MoS<sub>2</sub> in the near-infrared range, but the latter displays more significant absorption in the ultraviolet range. They can thus be applied effectively in different scenes. As a whole, these results make up for the shortage of monolayer 2D materials in optical characteristics and are beneficial for optoelectronic devices with the need for light absorption enhancement and absorption range broadening.

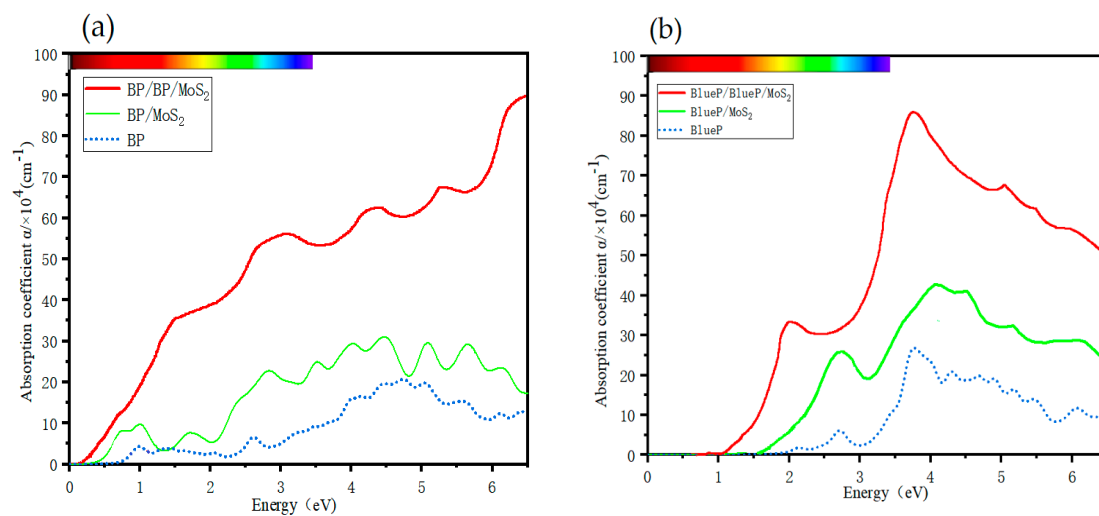


**Figure 5.** Optical absorption coefficient of (a) monolayer BP and MoS<sub>2</sub>, bilayer BP, BP/MoS<sub>2</sub> and BP/BP/MoS<sub>2</sub>; and (b) monolayer BlueP and MoS<sub>2</sub>, bilayer BlueP, BP/MoS<sub>2</sub> and BlueP/BlueP/MoS<sub>2</sub>.

Figure 6 displays the absorption coefficients of bilayer heterostructures graphene/BP, graphene/BlueP and graphene/MoS<sub>2</sub>, and the trilayer heterostructures BP/graphene/MoS<sub>2</sub> and BlueP/graphene/MoS<sub>2</sub>. The inset shows that the two kinds of trilayer heterostructures have stronger light absorption in the range below 0.8 eV than the related bilayer heterostructures, so they are better choices for graphene-based 2D materials to realize photodetectors widely responding to short-, mid- and long-wave infrared light. In the range of 2.2–6 eV, BP/graphene/MoS<sub>2</sub> shows remarkably higher light absorption than the related bilayer heterostructures, making it able to realize better graphene-based optoelectronic devices working in a wide range from visible to deep ultraviolet. BlueP/graphene/MoS<sub>2</sub> shows better light absorption characteristics than the related bilayer heterostructures in the range of 4–6 eV, so it is more suitable for use as a graphene-based solar-blind ultraviolet photodetector. These asymmetric graphene-sandwiched vdW heterostructures are thus proved to be effective in tuning and improving the performance of graphene-based 2D materials on the basis of guaranteeing the excellent electronic properties of graphene.

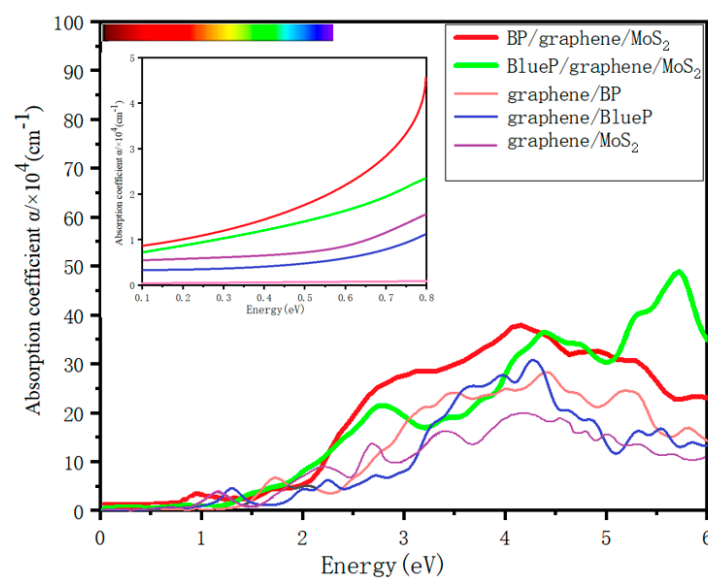


**Figure 6.** Optical absorption coefficient of BP/graphene/MoS<sub>2</sub> and BlueP/graphene/MoS<sub>2</sub> heterostructures, and the optical absorption coefficient of graphene/BP, graphene/BlueP and graphene/MoS<sub>2</sub> are also shown for comparison.

#### 4. Conclusions

Using the first-principles calculation based on DFT theory, we proposed and simulated trilayer 2D vdW heterostructures: BP/BP/MoS<sub>2</sub>, BlueP/BlueP/MoS<sub>2</sub>, BP/graphene/MoS<sub>2</sub> and BlueP/graphene/MoS<sub>2</sub>. The atomic structures of these heterostructures are all stable and look feasible to prepare. For BP/BP/MoS<sub>2</sub> and BlueP/BlueP/MoS<sub>2</sub>, all the bandgaps were tuned to be smaller, to effectively compensate for the shortage of corresponding monolayers and to satisfy a wider spectrum of applications with respect to the bilayer structures BP/MoS<sub>2</sub> and BlueP/MoS<sub>2</sub>, respectively. Their higher DOS, much stronger light absorption and more obvious type-II band alignment will realize better performance of optoelectronic devices working in a wide spectrum from mid-wave (short-wave) infrared to violet. In contrast, for BP/graphene/MoS<sub>2</sub> and BlueP/graphene/MoS<sub>2</sub>, most of the bandgaps were enlarged, implying different tuning mechanisms related to vdW interaction. Specifically in BP/graphene/MoS<sub>2</sub>, the graphene bandgap was well opened to 0.051 eV, more than one order of magnitude larger than usual, indicating more space for graphene tuning in trilayer vdW heterostructures. Accompanying the bandgap increase, both BP/graphene/MoS<sub>2</sub> and BlueP/graphene/MoS<sub>2</sub> exhibit absorption enhancement in wide spectral ranges, suggesting that these trilayer vdW heterostructures show better prospects as graphene-based 2D material optoelectronic devices with broad responses in the short- to long-wave infrared, visible to deep ultraviolet and solar-blind ultraviolet bands. It is concluded that the proposed 2D trilayer vdW heterostructures are potentially applicable as novel optoelectronic devices.

**Author Contributions:** B.C.: model building, simulation, data processing, and writing—original draft; Y.Z., R.J., X.W., S.H., X.H., W.Z., Q.D. and L.Z.: investigation help and discussion; P.L.: simulation instruction, discussion and revision guidance; H.-Z.S.: writing and revision guidance, project administration, resources, and supervision. All authors have read and agreed to the published version of the manuscript.

**Funding:** This research was supported by the National Key Research and Development Program of China under grants No. 2019YFB2203400 and No. 2021YFA0718803, and by the Natural Science Foundation of Sichuan Province under grant No. 2022NSFSC1817. We also acknowledge the support of the Special Subject of Significant Science and Technology of Sichuan Province under grant 2018TZDZX0001 and the Special Subject of Significant Innovation of Chengdu City under grant 2021-YF08-00159-GX.

**Data Availability Statement:** The data presented in this study are available on request from the corresponding author.

**Conflicts of Interest:** The authors declare no conflict of interest.

#### References

1. Miao, J.; Wang, C. Avalanche photodetectors based on two-dimensional layered materials. *Nano Res.* **2021**, *14*, 1878–1888. [[CrossRef](#)]
2. Liu, Y.; Weiss, N.O.; Duan, X.; Cheng, H.C.; Huang, Y.; Duan, X. Van der Waals heterostructures and devices. *Nat. Rev. Mater.* **2016**, *1*, 16042. [[CrossRef](#)]
3. Das, S.; Gulotty, R.; Sumant, A.V.; Roelofs, A. All two-dimensional, flexible, transparent, and thinnest thin film transistor. *Nano Lett.* **2014**, *14*, 2861–2866. [[CrossRef](#)] [[PubMed](#)]
4. Long, M.; Wang, P.; Fang, H.; Hu, W. Progress, challenges, and opportunities for 2D material based photodetectors. *Adv. Funct. Mater.* **2019**, *29*, 1803807. [[CrossRef](#)]
5. Akinwande, D.; Huyghebaert, C.; Wang, C.H.; Serna, M.I.; Goossens, S.; Li, L.J.; Koppens, F.H. Graphene and two-dimensional materials for silicon technology. *Nature* **2019**, *573*, 507–518. [[CrossRef](#)] [[PubMed](#)]
6. Geim, A.K.; Grigorieva, I.V. Van der Waals heterostructures. *Nature* **2013**, *499*, 419–425. [[CrossRef](#)]
7. Novoselov, K.S.; Mishchenko, O.A.; Carvalho, O.A.; Castro Neto, A.H. 2D materials and van der Waals heterostructures. *Science* **2016**, *353*, aac9439. [[CrossRef](#)]
8. Jariwala, D.; Marks, T.J.; Hersam, M.C. Mixed-dimensional van der Waals heterostructures. *Nat. Mater.* **2017**, *16*, 170–181. [[CrossRef](#)]
9. Wang, H.; Li, Z.; Li, D.; Chen, P.; Pi, L.; Zhou, X.; Zhai, T. Van der Waals Integration Based on Two-Dimensional Materials for High-Performance Infrared Photodetectors. *Adv. Funct. Mater.* **2021**, *31*, 2103106. [[CrossRef](#)]

10. Wang, P.; Xia, H.; Li, Q.; Wang, F.; Zhang, L.; Li, T.; Hu, W. Sensing infrared photons at room temperature: From bulk materials to atomic layers. *Small* **2019**, *15*, 1904396. [[CrossRef](#)]
11. Guan, X.; Yu, X.; Periyangounder, D.; Benzigar, M.R.; Huang, J.K.; Lin, C.H.; Wu, T. Recent progress in short-to long-wave infrared photodetection using 2D materials and heterostructures. *Adv. Opt. Mater.* **2021**, *9*, 2001708. [[CrossRef](#)]
12. Rogalski, A.; Antoszewski, J.; Faraone, L. Third-generation infrared photodetector arrays. *J. Appl. Phys.* **2009**, *105*, 344–348. [[CrossRef](#)]
13. Rhodes, D.; Chae, S.H.; Ribeiro-Palau, R.; Hone, J. Disorder in van der Waals heterostructures of 2D materials. *Nat. Mater.* **2019**, *18*, 541–549. [[CrossRef](#)] [[PubMed](#)]
14. Geim, A.K.; Novoselov, K.S. The rise of graphene. *Nat. Mater.* **2007**, *6*, 183–191. [[CrossRef](#)]
15. Bhimanapati, G.R.; Lin, Z.; Meunier, V.; Jung, Y.; Cha, J.; Das, S.; Robinson, J.A. Recent advances in two-dimensional materials beyond graphene. *ACS Nano* **2015**, *9*, 11509–11539. [[CrossRef](#)]
16. Ebnonnasir, A.; Narayanan, B.; Kodambaka, S.; Ciobanu, C.V. Tunable MoS<sub>2</sub> bandgap in MoS<sub>2</sub>-graphene heterostructures. *Appl. Phys. Lett.* **2014**, *105*, 031603. [[CrossRef](#)]
17. Radisavljevic, B.; Radenovic, A.; Brivio, J.; Giacometti, V.; Kis, A. Single-layer MoS<sub>2</sub> transistors. *Nat. Nanotechnol.* **2011**, *6*, 147–150. [[CrossRef](#)]
18. Zong, X.; Hu, H.; Ouyang, G.; Wang, J.; Shi, R.; Zhang, L.; Chen, X. Black phosphorus-based van der Waals heterostructures for mid-infrared light-emission applications. *Light Sci. Appl.* **2020**, *9*, 114. [[CrossRef](#)]
19. Chen, P.; Li, N.; Chen, X.; Ong, W.J.; Zhao, X. The rising star of 2D black phosphorus beyond graphene: Synthesis, properties and electronic applications. *2d Mater.* **2017**, *5*, 014002. [[CrossRef](#)]
20. Castellanos-Gomez, A. Black phosphorus: Narrow gap, wide applications. *J. Phys. Chem. Lett.* **2015**, *6*, 4280–4291. [[CrossRef](#)]
21. Zhao, X.; Bo, M.; Huang, Z.; Zhou, J.; Peng, C.; Li, L. Heterojunction bond relaxation and electronic reconfiguration of WS<sub>2</sub>-and MoS<sub>2</sub>-based 2D materials using BOLS and DFT. *Appl. Surf. Sci.* **2018**, *462*, 508–516. [[CrossRef](#)]
22. Hu, W.; Wang, T.; Zhang, R.; Yang, J. Effects of interlayer coupling and electric fields on the electronic structures of graphene and MoS<sub>2</sub> heterobilayers. *J. Mater. Chem. C* **2016**, *4*, 1776–1781. [[CrossRef](#)]
23. Le, N.B.; Huan, T.D.; Woods, L.M. Interlayer interactions in van der Waals heterostructures: Electron and phonon properties. *ACS Appl. Mater. Interfaces* **2016**, *8*, 6286–6292. [[CrossRef](#)] [[PubMed](#)]
24. Cai, Y.; Zhang, G.; Zhang, Y.W. Electronic properties of phosphorene/graphene and phosphorene/hexagonal boron nitride heterostructures. *J. Phys. Chem. C* **2015**, *119*, 13929–13936. [[CrossRef](#)]
25. Su, J.; Xiao, B.; Jia, Z. A first principle study of black phosphorene/N-doped graphene heterostructure: Electronic, mechanical and interface properties. *Appl. Surf. Sci.* **2020**, *528*, 146962. [[CrossRef](#)]
26. Behera, S.K.; Deb, P. Controlling the bandgap in graphene/h-BN heterostructures to realize electron mobility for high performing FETs. *RSC Adv.* **2017**, *7*, 31393–31400. [[CrossRef](#)]
27. Komsa, H.P.; Krasheninnikov, A.V. Electronic structures and optical properties of realistic transition metal dichalcogenide heterostructures from first principles. *Phys. Rev. B* **2013**, *88*, 085318. [[CrossRef](#)]
28. Lu, N.; Guo, H.; Li, L.; Dai, J.; Wang, L.; Mei, W.N.; Zeng, X.C. MoS<sub>2</sub>/MX<sub>2</sub> heterobilayers: Bandgap engineering via tensile strain or external electrical field. *Nanoscale* **2014**, *6*, 2879–2886. [[CrossRef](#)]
29. Ren, K.; Sun, M.; Luo, Y.; Wang, S.; Yu, J.; Tang, W. First-principle study of electronic and optical properties of two-dimensional materials-based heterostructures based on transition metal dichalcogenides and boron phosphide. *Appl. Surf. Sci.* **2019**, *476*, 70–75. [[CrossRef](#)]
30. Wang, S.; Tian, H.; Ren, C.; Yu, J.; Sun, M. Electronic and optical properties of heterostructures based on transition metal dichalcogenides and graphene-like zinc oxide. *Sci. Rep.* **2018**, *8*, 12009. [[CrossRef](#)]
31. Huang, L.; Li, J. Tunable electronic structure of black phosphorus/blue phosphorus van der Waals pn heterostructure. *Appl. Phys. Lett.* **2016**, *108*, 083101. [[CrossRef](#)]
32. Sun, M.; Chou, J.-P.; Yu, J.; Tang, W. Electronic properties of blue phosphorene/graphene and blue phosphorene/graphene-like gallium nitride heterostructures. *Phys. Chem. Chem. Phys.* **2017**, *19*, 17324–17330. [[CrossRef](#)] [[PubMed](#)]
33. Liao, C.; Zhao, Y.; Ouyang, G. Strain-modulated band engineering in two-dimensional black phosphorus/MoS<sub>2</sub> van der Waals heterojunction. *ACS Omega* **2018**, *3*, 14641–14649. [[CrossRef](#)] [[PubMed](#)]
34. Huang, L.; Huo, N.; Li, Y.; Chen, H.; Yang, J.; Wei, Z.; Li, S.S. Electric-field tunable band offsets in black phosphorus and MoS<sub>2</sub> van der Waals pn heterostructure. *J. Phys. Chem. Lett.* **2015**, *6*, 2483–2488. [[CrossRef](#)] [[PubMed](#)]
35. Tang, K.; Qi, W.; Li, Y.; Wang, T. Electronic properties of van der Waals heterostructure of black phosphorus and MoS<sub>2</sub>. *J. Phys. Chem. C* **2018**, *122*, 7027–7032. [[CrossRef](#)]
36. You, B.; Wang, X.; Zheng, Z.; Mi, W. Black phosphorene/monolayer transition-metal dichalcogenides as two dimensional van der Waals heterostructures: A first-principles study. *Phys. Chem. Chem. Phys.* **2016**, *18*, 7381–7388. [[CrossRef](#)]
37. Yang, F.; Han, J.; Zhang, L.; Tang, X.; Zhuo, Z.; Tao, Y.; Dai, Y. Adjustable electronic and optical properties of BlueP/MoS<sub>2</sub> van der Waals heterostructure by external strain: A First-principles study. *Nanotechnology* **2020**, *31*, 375706. [[CrossRef](#)]
38. Ye, L.; Li, H.; Chen, Z.; Xu, J. Near-infrared photodetector based on MoS<sub>2</sub>/black phosphorus heterojunction. *ACS Photonics* **2016**, *3*, 692–699. [[CrossRef](#)]
39. Liu, Y.; Shivananju, B.N.; Wang, Y.; Zhang, Y.; Yu, W.; Xiao, S.; Bao, Q. Highly efficient and air-stable infrared photodetector based on 2D layered graphene–black phosphorus heterostructure. *ACS Appl. Mater. Interfaces* **2017**, *9*, 36137–36145. [[CrossRef](#)]

40. Li, R. Electronic properties of hybrid graphene/nitrogen/graphene hetero-trilayers. *Phys. E Low-Dimens. Syst. Nanostructures* **2020**, *123*, 114166. [[CrossRef](#)]
41. Liu, B.; Chen, Y.; You, C.; Liu, Y.; Kong, X.; Li, J.; Zhang, Y. High performance photodetector based on graphene/MoS<sub>2</sub>/graphene lateral heterostructure with Schottky junctions. *J. Alloys Compd.* **2019**, *779*, 140–146. [[CrossRef](#)]
42. Datta, K.; Khosru, Q.D. Electronic properties of MoS<sub>2</sub>/MX<sub>2</sub>/MoS<sub>2</sub> trilayer heterostructures: A first principle study. *ECS J. Solid State Sci. Technol.* **2016**, *5*, Q3001–Q3007. [[CrossRef](#)]
43. Datta, K.; Shadman, A.; Rahman, E.; Khosru, Q.D.M. Trilayer TMDC Heterostructures for MOSFETs and Nanobiosensors. *J. Electron. Mater.* **2017**, *46*, 1248–1260. [[CrossRef](#)]
44. Bafekry, A.; Yagmurcukardes, M.; Akgenc, B.; Ghergherehchi, M.; Nguyen, C.V. Van der Waals heterostructures of MoS<sub>2</sub> and Janus MoSSe monolayers on graphitic boron-carbon-nitride (BC<sub>3</sub>, C<sub>3</sub>N, C<sub>3</sub>N<sub>4</sub> and C<sub>4</sub>N<sub>3</sub>) nanosheets: A first-principles study. *J. Phys. D: Appl. Phys.* **2020**, *53*, 355106. [[CrossRef](#)]
45. Liu, S.; Li, X.; Meng, D.; Li, S.; Chen, X.; Hu, T. Tunable electronic properties of MoS<sub>2</sub>/SiC heterostructures: A First-Principles study. *J. Electron. Mater.* **2022**, *51*, 3714–3726. [[CrossRef](#)]
46. Han, J.; Yang, F.; Xu, L.; Zhuo, Z.; Cao, X.; Tao, Y.; Liu, W. Modulated electronic and optical properties of bilayer/trilayer Blue Phosphorene/MoX<sub>2</sub> (X= S, Se) van der Waals heterostructures. *Surf. Interfaces* **2021**, *25*, 101228. [[CrossRef](#)]
47. Kim, D.; Hashmi, A.; Hwang, C.; Hong, J. Thickness dependent band gap and effective mass of BN/graphene/BN and graphene/BN/graphene heterostructures. *Surf. Sci.* **2013**, *610*, 27–32. [[CrossRef](#)]
48. Farooq, M.U.; Hashmi, A.; Hong, J. Thickness dependent optical properties of multilayer BN/graphene/BN. *Surf. Sci.* **2015**, *634*, 25–30. [[CrossRef](#)]
49. Xu, L.; Huang, W.Q.; Hu, W.; Yang, K.; Zhou, B.X.; Pan, A.; Huang, G.F. Two-dimensional MoS<sub>2</sub>-graphene-based multilayer van der Waals heterostructures: Enhanced charge transfer and optical absorption, and electric-field tunable Dirac point and band gap. *Chem. Mater.* **2017**, *29*, 5504–5512. [[CrossRef](#)]
50. Xia, C.; Du, J.; Fang, L.; Li, X.; Zhao, X.; Song, X.; Wang, T.; Li, J. PtSe<sub>2</sub>/graphene hetero-multilayer: Gate-tunable Schottky barrier height and contact type. *Nanotechnology* **2018**, *29*, 465707. [[CrossRef](#)]
51. Long, M.; Liu, E.; Wang, P.; Gao, A.; Xia, H.; Luo, W.; Miao, F. Broadband photovoltaic detectors based on an atomically thin heterostructure. *Nano Lett.* **2016**, *16*, 2254–2259. [[CrossRef](#)] [[PubMed](#)]
52. Li, A.; Chen, Q.; Wang, P.; Gan, Y.; Qi, T.; Wang, P.; Gong, Y. Ultrahigh-sensitive broadband photodetectors based on dielectric shielded MoTe<sub>2</sub>/Graphene/SnS<sub>2</sub> p–g–n junctions. *Adv. Mater.* **2019**, *31*, 1805656. [[CrossRef](#)] [[PubMed](#)]
53. Sun, G.; Kürti, J.; Rajczy, P.; Kertesz, M.; Hafner, J.; Kresse, G. Performance of the Vienna ab initio simulation package (VASP) in chemical applications. *J. Mol. Struct. THEOCHEM* **2003**, *624*, 37–45. [[CrossRef](#)]
54. Hafner, J. Ab-initio simulations of materials using VASP: Density-functional theory and beyond. *J. Comput. Chem.* **2008**, *29*, 2044–2078. [[CrossRef](#)] [[PubMed](#)]
55. Bucko, T.; Hafner, J.; Lebegue, S.; Angyan, J.G. Improved description of the structure of molecular and layered crystals: Ab initio DFT calculations with van der Waals corrections. *J. Phys. Chem. A* **2010**, *114*, 11814–11824. [[CrossRef](#)]
56. Klimeš, J.; Bowler, D.R.; Michaelides, A. Chemical accuracy for the van der Waals density functional. *J. Phys. Condens. Matter* **2010**, *22*, 022201. [[CrossRef](#)]
57. Dong, H.M.; Huang, L.S.; Liu, J.L.; Huang, F.; Zhao, C.X. Layer-dependent optoelectronic properties of black phosphorus. *Int. J. Mod. Phys. C* **2020**, *31*, 2050177. [[CrossRef](#)]
58. Sun, M.; Chou, J.P.; Gao, J.; Cheng, Y.; Hu, A.; Tang, W.; Zhang, G. Exceptional optical absorption of buckled arsenene covering a broad spectral range by molecular doping. *ACS Omega* **2018**, *3*, 8514–8520. [[CrossRef](#)]
59. Yu, L.; Lee, Y.H.; Ling, X.; Santos, E.J.; Shin, Y.C.; Lin, Y.; Palacios, T. Graphene/MoS<sub>2</sub> hybrid technology for large-scale two-dimensional electronics. *Nano Lett.* **2014**, *14*, 3055–3063. [[CrossRef](#)]
60. Zhang, J.L.; Zhao, S.; Han, C.; Wang, Z.; Zhong, S.; Sun, S.; Guo, R.; Zhou, X.; Gu, C.D.; Yuan, K.D.; et al. Epitaxial growth of single layer blue phosphorus: A new phase of two-dimensional phosphorus. *Nano Lett.* **2016**, *16*, 4903–4908. [[CrossRef](#)]
61. Qiao, J.; Kong, X.; Hu, Z.X.; Yang, F.; Ji, W. High-mobility transport anisotropy and linear dichroism in few-layer black phosphorus. *Nat. Commun.* **2014**, *5*, 4475. [[CrossRef](#)] [[PubMed](#)]
62. Yan, J.; Kim, M.H.; Elle, J.A.; Sushkov, A.B.; Jenkins, G.S.; Milchberg, H.M.; Fuhrer, M.S.; Drew, H.D. Dual-gated bilayer graphene hot-electron bolometer. *Nat. Nanotechnol.* **2012**, *7*, 472–478. [[CrossRef](#)] [[PubMed](#)]
63. Kim, J.D.; Chen, X.; Li, X.; Coleman, J.J. Photocurrent density enhancement of a III-V inverse quantum dot intermediate band gap photovoltaic device. In Proceedings of the 2015 Conference on Lasers and Electro-Optics (CLEO), San Jose, CA, USA, 10–15 May 2015.
64. Joseph, I.; Wan, K.; Hussain, S.; Guo, L.; Xie, L.; Shi, X. Interlayer angle-dependent electronic structure and optoelectronic properties of BP-MoS<sub>2</sub> heterostructure: A first principle study. *Comput. Mater. Sci.* **2021**, *186*, 110056. [[CrossRef](#)]

**Disclaimer/Publisher's Note:** The statements, opinions and data contained in all publications are solely those of the individual author(s) and contributor(s) and not of MDPI and/or the editor(s). MDPI and/or the editor(s) disclaim responsibility for any injury to people or property resulting from any ideas, methods, instructions or products referred to in the content.